applied sciences

Article

Effects of Polyurethane Absorber for Improving the Contrast between Fascia and Muscle in Diagnostic Ultrasound Images

Chan-Sol Park [1], Soo-Jin Ahn [2], Yeong-Bae Lee [3,4,*] and Chang-Ki Kang [1,2,3,*]

1 Department of Health Science, Gachon University Graduate School, Incheon 21936, Republic of Korea; cs11111kr@gachon.ac.kr
2 Department of Radiological Science, College of Health Science, Gachon University, Incheon 21936, Republic of Korea
3 Neuroscience Research Institute, Gachon University, Incheon 21565, Republic of Korea
4 Department of Neurology, Gil Medical Center, Gachon University College of Medicine, Incheon 21565, Republic of Korea
* Correspondence: yeongbaelee@gachon.ac.kr (Y.-B.L.); ckkang@gachon.ac.kr (C.-K.K.)

Abstract: In ultrasound diagnostics, acoustic absorbers block unwanted acoustic energy or prevent the reception of echo signals from structures outside the target area. Non-metallic absorbers provide a low-echoic signal that is suitable for observing the anatomy of the area to which the absorber is attached. In this study, we aimed to evaluate the effect of a polyurethane film absorber (PU) on ultrasound diagnostic imaging and investigate its effectiveness in improving the image contrast between the fascia and muscle structures. Twenty-six healthy men in their twenties participated in this study. The experiment was performed with the participant in the supine position and with an ultrasound transducer probe placed at the center of the measurement area on the abdomen. Images of the rectus abdominis (RA; muscle) and rectus sheath, e.g., fascia including superficial fascia (SF) and deep fascia (DF), obtained after attaching a PU, were compared with those obtained without the absorber (No_PU). The thickness was measured using brightness mode ultrasound imaging. To analyze the quantitative differences in the fascia and muscle images depending on the presence of the absorber, the signal-to-noise ratio (SNR) and contrast-to-noise ratio (CNR) were derived from the signal intensities measured in the target areas. The thickness of the fascia and muscle was similar in all regions of interest, regardless of the absorber; therefore, the existing diagnostic value was maintained. Overall, the signal intensity decreased; however, the SNRs of the RA, SF, and DF differed significantly. The SNR of the RA decreased in the PU but increased for the SF and DF. The CNRs for SF-RA and DF-RA significantly increased with the PU. In this study, we demonstrated that the PU behaved similarly to previously used metallic absorbers, reducing the signal from the attachment site while accurately indicating the attachment site in the ultrasound images. Furthermore, the results showed that the PU efficiently distinguished fascia from surrounding tissues, which could support studies requiring increased signal contrast between fascia and muscle tissue and aid the clinical diagnosis of fascial diseases.

Keywords: ultrasound imaging; polyurethane; absorber; rectus abdominis; rectus sheath

check for updates

Citation: Park, C.-S.; Ahn, S.-J.; Lee, Y.-B.; Kang, C.-K. Effects of Polyurethane Absorber for Improving the Contrast between Fascia and Muscle in Diagnostic Ultrasound Images. *Appl. Sci.* **2024**, *14*, 2126. https://doi.org/10.3390/app14052126

Academic Editors: Laura Peralta and Kirsten Christensen-Jeffries

Received: 25 January 2024
Revised: 22 February 2024
Accepted: 29 February 2024
Published: 4 March 2024

1. Introduction

Ultrasound (US) is a mechanical wave generated by the piezoelectric effect of piezoelectric elements that constitute an ultrasonic transducer. The waves transmitted from the transducer interact with the medium through absorption, scattering, and attenuation depending on the characteristics of the medium, such as density and acoustic impedance. After going through these processes, the waves reflected to the transducer are utilized [1–3]. When US interacts with an elastic medium, the propagation is attenuated due to scattering, refraction, and absorption, reducing the amplitude and intensity of the wave as it passes through the medium [4,5]. The penetration depth is affected by the frequency of the ultrasonic wave. This phenomenon increases the attenuation at high frequencies and reduces the penetration depth. Conversely, at lower frequencies, attenuation decreases and the penetration depth increases [6].

Owing to these characteristics, US is used in various fields in both industry and medicine. In the medical field, US aids diagnosis by providing images of the body using reflected wave signals through computer processing. Compared to computed tomography (CT) and magnetic resonance imaging (MRI) examinations, US diagnosis is characterized by requiring less radiation exposure, enabling real-time examination, and/or having a short scanning time. Moreover, US imaging exhibits high reliability and significance when compared to CT or MRI [7–9]. Diagnostic US imaging methods include a brightness mode (B-mode) that expresses the intensity of the echo in grayscale and a motion mode (M-mode) that detects temporal motion. In addition, there are color and power Doppler modes that visualize blood flow direction and speed information using the color spectrum, and each method facilitates clinical diagnosis according to the purpose of the examination [10–12].

The image brightness can be adjusted in various ways, using artifacts, parameter adjustments, and auxiliary devices [13,14]. Methods that use artifacts include the needle guidance method that uses shadowing artifacts, which are shadows generated by metallic materials [15]. The imaging parameters can also change the brightness of an image by adjusting the time-gain-compensation (TGC) or gain [16,17]. The brightness of an application area can also be adjusted using auxiliary devices such as gel pads or absorbers [18,19]. The gel pad brightens the region of interest (ROI), whereas the absorber confirms the location of the application area in the image by darkening the ROI, and is used in studies of the musculoskeletal system, rehabilitation, and sports [19–22]. Recently, as interest in health has increased, the number of people exercising has increased, and research on effective exercise methods is underway. In addition to functional research on muscles to improve exercise capacity, research on fascia is also being conducted. In particular, various modified exercise methods for the rectus abdominis (RA; muscle) were introduced. The RA is surrounded by fascia called the rectus sheath. In the diagnosis image, the rectus sheath is called superficial fascia (SF) on the ventral side and deep fascia (DF) on the dorsal side, and various studies regarding hematomas that occur in the rectus sheath have been conducted [23]. Fascia is a connective tissue that surrounds bones, nerves, blood vessels, and muscles and is distributed throughout the body [24]. Damage to the fascia can cause dysfunction and pain in the corresponding area, requiring appropriate diagnosis and treatment [24]. Marking the ROI using an absorber in the diagnostic US is a method in which the ROI signal is darkened using artifacts. Studies have used metals such as aluminum, as well as non-metallic materials such as rubber, leather, and polyurethane [25–27]. In particular, the acoustic impedance (Z) of aluminum is 17.33 MRayls, so the impedance mismatch at the boundary of aluminum and skin (Z = 1.53 to 1.68 Mrayls) causes acoustic shadow artifacts that appear as anechoic signals in the image, causing the aluminum to act as an absorber [28]. However, in US images, tissues at the attachment site are not observed because of these acoustic artifacts, and the skin surface at the attachment site is also covered with an opacity absorber, which hinders the confirmation of the attachment site with the naked eye [28,29]. Additionally, the risk of injury when using thin aluminum requires caution. However, polyurethane, which is a non-metallic material, has a Z of 1.80 MRayls, resulting in a lower Z difference with the skin than that of aluminum [28]. Furthermore, the degree of acoustic shadow artifacts is low; therefore, it is hypoechoic in the image [22]. Thus, in diagnostic US images, both metallic and non-metallic absorbers can aid in controlling the signal intensity from anechoic to hypoechoic because of the Z difference between the body tissues and the absorber.

With the advent of various non-metallic materials, materials that are suitable as absorbents are becoming increasingly diverse. In particular, the transparent nature of polyurethane allows visual confirmation of its attachment site on the skin [22,28]. In addition, it can be manufactured in various shapes and as thin biomedical phantoms [30,31], exhibits elasticity and waterproofing properties, and serves as a dressing tool to prevent infection in wounds through a sterile dressing tool [32,33]. Polyurethane is characterized by a high degree of safety because it is consumable in existing clinical practice and can also act as an absorber in US diagnosis.

However, despite the use of various types of absorbers, most absorbers use metals and involve the risk of allergies and injuries. Recently, non-metallic absorbers have been used to compensate for the shortcomings of these metals. Because low-echoic images can be confirmed at the location of the absorber, new ways to use them as absorbers must be devised. In addition, because metal absorbers appear anechoic, no research has been conducted to evaluate the signal intensity in images. However, polyurethane is non-metallic and appears hypoechoic; therefore, the changes in signal intensities in images can be compared.

In this study, we examined the efficiency of distinguishing between the fascia and surrounding tissues and evaluated a new function to confirm the location of the absorber by adding shading to the image. A polyurethane absorber (PU) was attached to the RA, a large, long, and flat muscle of the abdomen comprising various tissues, and US images were obtained to compare and quantitatively analyze the changes in the signal intensities of the fascia and muscle depending on whether the absorber was used.

2. Materials and Methods

2.1. Participants

This study was approved by the Institutional Review Board (IRB: 1044396-202105-HR-105-01) for experimental safety and effectiveness, and 26 healthy men in their twenties (age: 23.81 $\pm$ 2.17 years [mean $\pm$ standard deviation, SD]; height: 175.00 $\pm$ 5.89 cm; weight: 73.23 $\pm$ 8.51 kg) participated in this study after providing written informed consent. Participants with no history of abdominal diseases or discomfort during US measurements were selected.

2.2. Experiments and Data Acquisition

A diagnostic US device (RS85, Samsung Medison, Seoul, Republic of Korea) and a linear transducer array probe (LA2-14A, Samsung Medison, Seoul, Republic of Korea) with a frequency bandwidth of 2–14 MHz were used to acquire transverse B-mode scan images. The experiment was conducted with the participant in a supine position, and the transducer probe was placed in the center of the measurement area (5 cm above and 5 cm to the left of the navel) (Figure 1A). The measurement location was chosen based on information obtained from the pilot study in which the tendinous intersection was not observed in the US image [22]. The RA, SF, and DF were identified in the B-mode image (Figure 1B) and the corresponding area was marked with a blue pen on an absorptive marker on the skin (Figure 1A). The B-mode images were acquired without the absorber (No_PU). Subsequently, a transparent PU (Superfix BNG-#2003, BANDGOLD, Anyang, Republic of Korea) was cut into half the probe size (width: 30 mm, length: 10 mm, thickness: 0.05 mm) and attached to the right side of the measurement area to obtain B-mode images. The PU size and the location were determined to confirm the exact measurement location and to examine changes in signal intensity within the B-mode image. To prevent abdominal motion artifacts during the B-mode scanning, participants were asked to hold their breath for approximately 5 s, sufficient for localization and image acquisition. All participants underwent image acquisition for each attached and unattached absorber.

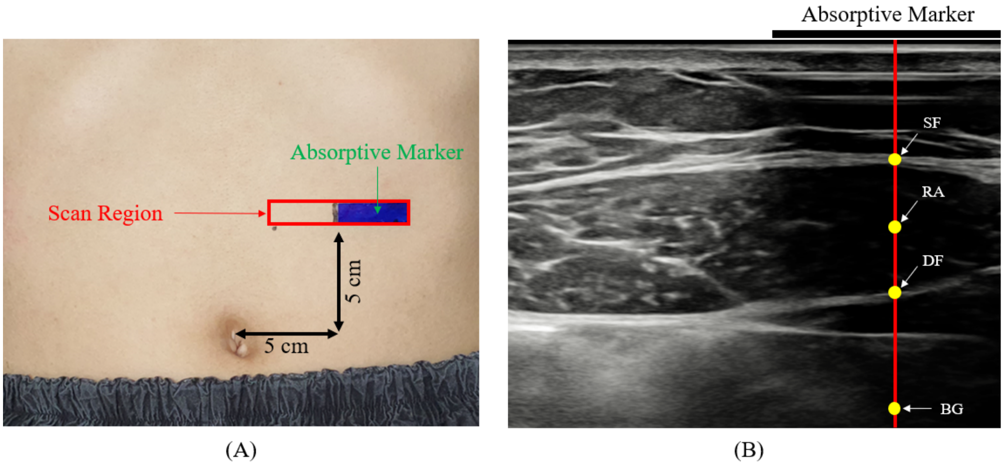

Figure 1. Absorptive marker and ultrasound image. (**A**) The scan region for the US imaging is shown in a red box and the location of the transparent absorptive marker is shown in blue. (**B**) The regions of interest are shown in yellow circles and the red vertical line is the midpoint of the absorber in the B-mode image, respectively.

The acquired US images were quantitatively evaluated based on the thickness, signal intensity, signal-to-noise ratio (SNR), and contrast-to-noise ratio (CNR) of the RA, SF, and DF. US images were acquired in DICOM format, and the thickness was measured using DICOM Viewer software (RadiAnt DICOM Viewer Version 2021.2.2 (64-bit), Medixant, Poznan, Poland, Eastern Europe). The thickness and signal intensity were measured at a vertical location one-quarter from the right edge of the B-mode image using the same evaluation protocol, corresponding to the central position of the absorber (as shown in the red vertical line in Figure 1). The thickness of SF and DF was measured where the vertical lines overlap, and the thickness of RA was measured at the bottom of SF and the top of DF. The signal intensity was measured at each location where RA, SF, and DF meet the vertical line, and the thickness of each tissue was measured using the full width at half maximum of the signal intensity within the vertical line. The signal intensity of the background (BG) was measured by setting the midpoint between DF and the bottom of the image.

The signal intensity was measured in the area corresponding to the center of the absorber on the right side of the image using an image analysis program (ImageJ version 1.52a, free software, https://imagej.net/ij, accessed on 2 March 2024). The mean signals and standard deviations (SD) of the RA, SF, and DF were measured. In addition, a BG region (a circle with a diameter of nine pixels) was selected for the SNR and CNR calculations, and its SD was measured (Figure 1B). The CNR of SF and DF were determined in contrast to RA, corresponding to SF-RA and DF-RA, respectively.

Using the mean signal intensity of the ROI and SD of the BG, the signal changes in the RA, SF, and DF with and without the absorber were compared with the SNR and CNR calculated using the following formulas:

$$\mathrm{SNR} = \frac{\text{Mean of signal}_{\mathrm{ROI}}}{\text{Standard Deviation}_{\mathrm{Background}}}, \tag{1}$$

$$\mathrm{CNR} = \frac{\text{Mean of signal}_{\mathrm{ROI\_A}} - \text{Mean of signal}_{\mathrm{ROI\_B}}}{\text{Standard Deviation}_{\mathrm{Background}}}. \tag{2}$$

2.3. Statistical Analysis

Statistical analysis of the measured values for each variable was performed using a statistical analysis program (Jamovi version 2.2.5, free software; https://www.jamovi.org, accessed on 2 March 2024). The measured thickness values were analyzed for reliability using the interclass correlation coefficient. A normality test was performed using the

Shapiro–Wilk test to analyze the differences in thickness, signal intensity, and the SNRs of RA, SF, and DF, and the CNRs of SF-RA and DF-RA depending on whether the absorber was attached or not. Subsequently, a paired sample *t*-test was performed to analyze the dependent variables. The mean difference was calculated by subtracting the means, for example, $\overline{X_1} - \overline{X_2}$, where the means of Factors 1 and 2 are $\overline{X_1}$ and $\overline{X_2}$, respectively. The standard error (SE) was calculated using the formula $E = \sqrt{SD_1{}^2/n_1 + SD_2{}^2/n_2}$, where the SD and sample sizes of Factors 1 and 2 are SD_1 and SD_2 and n_1 and n_2, respectively. The level of statistical significance was set at $p < 0.05$ for all statistical analyses.

3. Results

The changes in the thicknesses of the fascia and muscle according to absorber usage on B-mode images were compared using image analysis and statistical programs. When comparing the thicknesses of RA, SF, and DF, RA was 12.15 ± 2.73 mm and 11.64 ± 2.75 mm with No_PU and PU, respectively; however, no significant difference (p = 0.260) was observed. Likewise, the thicknesses for SF were 0.93 ± 0.28 mm and 0.89 ± 0.24 mm with No_PU and PU, respectively; however, the difference was insignificant (p = 0.318). For DF, the thicknesses were 0.89 ± 0.31 mm and 0.78 ± 0.21 mm with No_PU and PU, respectively; however, there was no significant difference (p = 0.122) (Table 1 and Figure 2). The inter-rater reliability of the thickness was high (Cronbach's α = 0.998).

Table 1. Comparison of the thickness for No_PU and PU.

			Mean	SD	Mean Difference (No_PU–PU)	SE	t Statistic	p
Thickness (mm)	RA	No_PU	12.15	2.73	0.511	0.442	1.16	0.260
		PU	11.64	2.75				
	SF	No_PU	0.93	0.28	0.045	0.044	1.02	0.318
		PU	0.89	0.24				
	DF	No_PU	0.89	0.31	0.111	0.069	1.60	0.122
		PU	0.78	0.21				

Abbreviations: DF, deep fascia; RA, rectus abdominis; SD, standard deviation; SE, standard error; SF, superficial fascia.

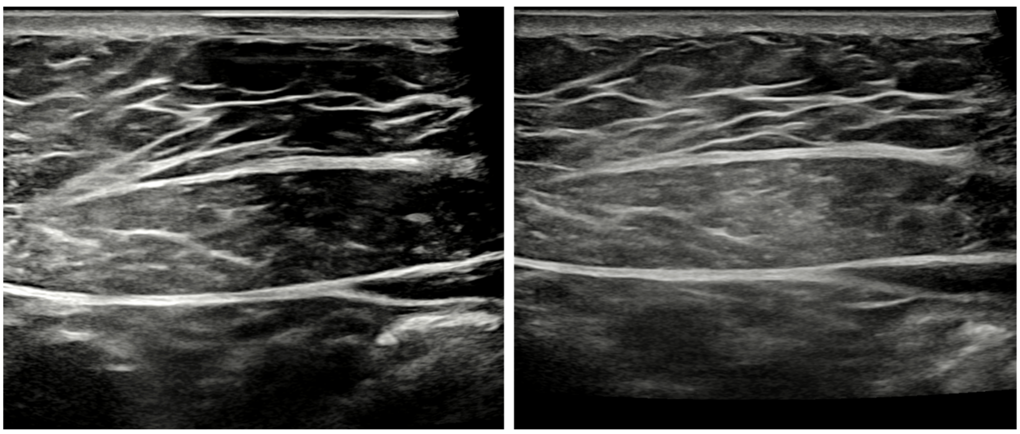

Figure 2. Ultrasound images of a representative subject with PU (**left**) and No_PU (**right**).

For RA, the signal intensities with No_PU and PU were 76.15 ± 15.08 and 12.41 ± 4.09, respectively, which showed a significant difference ($p < 0.001$). For SF, the signal intensities with No_PU and PU were 180.02 ± 16.53 and 106.26 ± 20.33, respectively, which also showed a significant difference ($p < 0.001$). For DF, the signal intensities with No_PU and PU were 154.90 ± 16.87 and 72.72 ± 20.39, respectively, which showed a significant difference ($p < 0.001$). For BG, the signal intensities with No_PU and PU were 53.04 ± 33.08 and 6.75 ± 5.84, respectively, which demonstrated a significant difference ($p < 0.001$) (Table 2).

Table 2. Comparison of the signal intensity for No_PU and PU.

			Mean	SD	Mean Difference (No_PU–PU)	SE	t Statistic	p
Signal intensity	RA	No_PU	76.15	30.91	63.7	6.17	10.33	<0.001 *
		PU	12.41	10.67				
	SF	No_PU	180.02	28.35	73.8	5.21	14.15	<0.001 *
		PU	106.26	39.72				
	DF	No_PU	154.90	43.02	82.2	7.75	10.60	<0.001 *
		PU	72.72	35.74				
	BG	No_PU	53.40	33.08	46.6	6.43	7.25	<0.001 *
		PU	6.75	5.84				

* $p < 0.05$. Abbreviations: BG, background; DF, deep fascia; RA, rectus abdominis; SD, standard deviation; SE, standard error; SF, superficial fascia.

For RA, the SNRs with No_PU and PU were 13.18 ± 5.21 and 5.82 ± 3.52, respectively, which demonstrated a significant difference ($p < 0.001$). For SF, the SNRs with No_PU and PU were 31.37 ± 10.73 and 67.07 ± 43.87, respectively, which exhibited a significant difference ($p < 0.001$). For DF, the SNRs with No_PU and PU were 25.64 ± 6.67 and 37.54 ± 22.23, respectively, which showed a significant difference ($p = 0.013$) (Table 3 and Figure 3).

Table 3. Comparison of the SNRs for No_PU and PU.

			Mean	SD	Mean Difference (No_PU–PU)	SE	t Statistic	p
SNR	RA	No_PU	13.18	5.21	−35.70	8.51	−4.20	<0.001 *
		PU	5.82	3.52				
	SF	No_PU	31.37	10.73	7.36	1.20	6.12	<0.001 *
		PU	67.07	43.87				
	DF	No_PU	25.64	6.67	−11.91	4.33	−2.75	0.013 *
		PU	37.54	22.23				

* $p < 0.05$. Abbreviations: DF, deep fascia; RA, rectus abdominis; SD, standard deviation; SE, standard error; SF, superficial fascia; SNR, signal-to-noise ratio.

For SF-RA, the values of the CNR were 16.70 ± 6.92 and 50.10 ± 26.38 with No_PU and PU, respectively, while for DF-RA, the values of the SNR were 12.30 ± 7.97 and 32.00 ± 22.53, with No_PU and PU, respectively. Both cases exhibited significant differences ($p < 0.001$ in each case) (Table 4 and Figure 3).

Table 4. Comparison of the CNR for No_PU and PU.

			Mean	SD	Mean Difference (No_PU–PU)	SE	t Statistic	p
CNR	SF-RA	No_PU	16.70	6.92	−33.40	5.38	−6.20	<0.001 *
		PU	50.10	26.38				
	DF-RA	No_PU	12.30	7.97	−19.70	4.59	−4.28	<0.001 *
		PU	32.00	22.53				

* $p < 0.05$. Abbreviations: CNR, contrast-to-noise ratio; DF, deep fascia; RA, rectus abdominis; SD, standard deviation; SE, standard error; SF, superficial fascia.

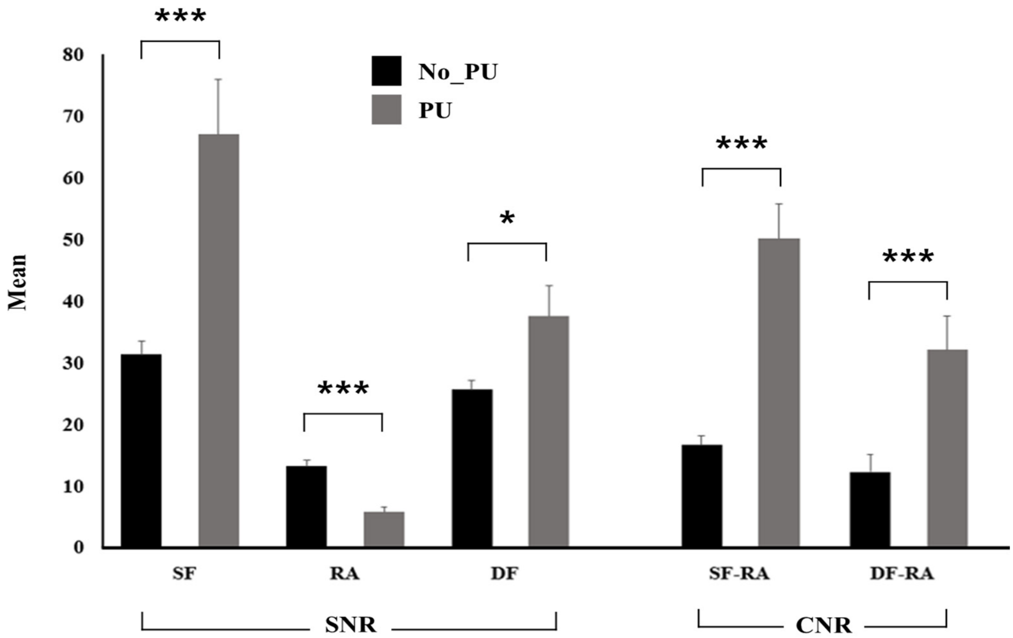

Figure 3. SNR and CNR changes in each tissue with PU and No_PU. The SNR and CNR show significant differences with PU when compared to No_PU ($p < 0.05$). * $p < 0.05$, *** $p < 0.001$.

4. Discussion

In the medical field, PU is used as a sterile dressing tool and is also manufactured to be used as a probe cover [32–34]. However, the PU for probe covers compensates for the entire image by adjusting parameters such as time-gain compensation and/or gain, making it difficult to investigate signal differences that occur locally in the image. On the other hand, PU absorbers can be used as markers for local areas and can complement the limitations of previously used metal absorbers. Therefore, this study investigated the changes in the signal intensity of US images depending on whether a PU was attached to the skin, at which point it could easily observe the RA, SF, and DF of the abdomen. The thicknesses and signal intensities of the RA, SF, and DF with the PU were compared with those corresponding to No_PU. The comparison showed that the thicknesses of the RA, SF, and DF with PU decreased by 4.20%, 5.37%, and 12.50%, respectively; however, the differences were not significant. No significant differences were observed in muscle thickness following the RA measurement protocol used in this study. In addition, in the No_PU image, the signal intensity of the SF and DF was much higher than that of the RA, and the hypoechoic signal appeared even when PU was attached, so there was no significant difference in the thickness of the SF and DF depending on the presence or absence of the absorber. Therefore, PU can be used for diagnostic US images, unlike conventional absorption materials such as aluminum and leather, which generate anechoic shadow owing to shadow artifacts [25,26].

However, the signal intensities of the RA, SF, DF, and BG with PU decreased by 40.97%, 53.05%, 83.70%, and 87.36%, respectively. This reduction occurs due to interactions between

PU and each body tissue, including attenuation and scattering due to differences of Z and/or density of the medium. In the case of a metallic absorber, the signal intensity decreases by nearly 100%, resulting in an anechoic image, but in the case of PU, a non-metallic absorber, a hypoechoic image appears. In particular, the amount of change in the BG signal, which is closely related to SNR and CNR, is mostly reduced, meaning that PU can act as an effective filter [35]. Various filtering methods through computer signal processing are being studied to remove noise, and by applying these filtering methods and PU together, an efficient noise improvement method can be developed [35,36].

The SNR of the RA with PU decreased by 55.90%, whereas those of the SF and DF increased by 46.41% and 113.80%, respectively, and were statistically different from those with No_PU. In the presence of the PU, all signal intensities in the RA, SF, and DF decreased by 83.70%, 41.03%, and 53.05%, respectively, while the SD of the BG decreased by 71.0%. Thus, the SNRs of SF and DF exhibited a greater increase owing to the greater reduction in the SD of BG. However, the SNR of the RA was reduced because of the substantial reduction in the signal intensity of the RA with the PU. This result indicates that the fascia can be easily observed by increasing the SNRs of SF and DF, which could be useful for diagnosing diseases such as necrosis that can affect the fascia.

For PU, the CNRs of SF-RA and DF-RA increased by 199.88% and 159.75%, respectively, and were statistically different from those of No_PU. The reduction in the signal intensity of the RA was relatively higher than that of the SF and DF in the PU; therefore, the CNR of the PU was higher than that of No_PU. This suggests that the fascia could be clearly observed owing to the increase in the CNRs of SF and DF relative to the RA. These results can promote the observation of the fascia in the image and increase the accuracy and efficiency of fascial lesion diagnosis.

To image fascia, MRI and a US B-mode scan can be used [37]. Recently, a method using elastography to study fascia function was introduced [38]. However, MRI has various limitations compared to US, such as the high cost and long scan time required. In addition, in the case of elastography using US, tissue elasticity is also provided as a numerical value, so there is no visual difference from existing B-mode images. In this study, the overall signal intensity decreased when the PU was attached; however, the SNR increased in the SF and DF and decreased in the RA. In addition, the signal intensity of RA was significantly lower compared to those of SF and DF, while the CNRs of SF-RA and DF-RA increased significantly. This result proves that when polyurethane is used as an absorber, the SNR and CNR can be increased without a difference in the thickness of the fascia and muscle; thus, the fascia can be observed more clearly in the US image. In most US equipment, parameters such as TGC and gain can be subjectively adjusted according to the operator's visual inspection. In particular, since TGC is divided into several parts depending on the imaging depth, it is difficult to accurately determine the appropriate parameters in detail. This means that a fine adjustment of parameters is limited to the structures localized within each part of the TGC. Unlike TGC, the gain parameter controls the brightness of the entire image and is difficult to fine-tune, so it is difficult to expect the simultaneous changes shown in the SNR and CNR when the PU is attached, as shown in the results of this study. Therefore, US images with the PU attached help distinguish between the fascia and tissues that exist in most body structures, and PU absorber images with improved clarity can be used for a variety of purposes, including identifying tissue boundaries, and calculating the length. This is because the fascia is a connective tissue that surrounds the tissues and organs of the body and serves to distinguish the boundaries between tissues and organs [39,40]. In particular, the fascia and surrounding tissues in fascial diseases, such as abdominal fascia pain syndrome and plantar fasciitis, can be easily distinguished when the PU is used for diagnosis using US images [41,42].

Moreover, a vascular-enhanced imaging method that uses microbubbles to identify blood vessels and flow using US is currently used [43,44]. The method using microbubbles can generate the enhanced and differentiated signals when microbubbles attach to blood vessels. However, it requires the invasive injection of microbubbles. Furthermore, microbubble imaging has limitations when applied to infants or patients with diseases, and also has side effects such as headaches, difficulty breathing, and chest pain [45]. However, images obtained using PU instead of microbubbles can also distinguish between blood vessels and tissues more quickly, non-invasively, and without side effects. Because fascia surrounds bones, nerves, and blood vessels, the SNR of fascia around blood vessels with PU may increase [24].

In clinical practice, during the treatment of tumors such as breast cancer, an absorber is used to determine the location of the tumor, and its location is tattooed with metal ink, or a metal capsule made of titanium is inserted into the body using a needle [46–48]. This can be confirmed as a metal artifact on X-ray, CT, MRI, and US images; however, because this is an invasive method, the side effects must be considered [46,49]. However, if the location is confirmed with a US image obtained using a non-invasively attached PU, radiation exposure can be reduced. Additionally, the PU can identify the attached area in the US image, which can help track the location of the tumor.

Therefore, polyurethane is expected to be used for various purposes, including its role as an existing marker in various diagnostic and imaging studies, by controlling the signal intensity. PU can act as an absorptive marker, reducing the signal intensity of the ROI and creating a hypoechoic area. This is a different characteristic from metallic absorbers, which display an anechoic signal. This means that the brightness of the area of interest where the PU absorber is attached can be also corrected through parameter adjustment, providing the optimal image for diagnosis without any additional change in US intensity. In particular, when attaching a PU absorber, the muscle signal is greatly reduced compared to the fascia signal, so it is possible to obtain images with the fascia further emphasized through adjusting parameters such as TGC or gain. In addition, diagnosis is often delayed because additional time is required when the original image is post-processed. However, in the case of PU absorbers, it is expected that rapid diagnosis will be possible because it can be confirmed through imaging at the same time as scanning without any additional post-processing. If a method for emphasizing signals in these specific areas is implemented with embedded software and real-time post-processing technology is developed, not only will fast and efficient diagnosis be possible, but various ultrasound technologies can be designed.

However, this study had some limitations. First, this study did not provide information on absorbers made from various materials. Second, it was limited to evaluating the fascia and muscles of the abdominal area. Thirdly, this study only checked the B-mode scan; thus, its applicability to other scanning methods could not be evaluated. Finally, this study was conducted only on young men, because men who are less sensitive to abdominal exposure may be of higher interest. Therefore, in future studies, various absorptive materials should be used, and the image quality should be quantitatively evaluated according to the material. In addition, the applicability of the absorber to other genders, age groups, and body parts, as well as the applicability to clinical surgeries such as needle guidance, must be ensured.

In conclusion, this study assessed the new role of a PU on the RA during US imaging. The results proved that the absorber may facilitate easy observation of the fascia and muscles. The results of this study may serve as the basis for developing diagnostic methods and absorbers that can help diagnose fascial diseases.

Author Contributions: Conceptualization, Y.-B.L. and C.-K.K.; methodology, Y.-B.L. and C.-K.K.; software, S.-J.A. and C.-S.P.; validation, Y.-B.L. and C.-K.K.; formal analysis, S.-J.A. and C.-S.P.; investigation, S.-J.A. and C.-S.P.; resources, Y.-B.L. and C.-K.K.; data curation, Y.-B.L. and C.-K.K.; writing—original draft preparation, S.-J.A. and C.-S.P.; writing—review and editing, Y.-B.L. and C.-K.K.; visualization, S.-J.A. and C.-S.P.; supervision, Y.-B.L. and C.-K.K.; project administration, Y.-B.L. and C.-K.K.; funding acquisition, Y.-B.L. and C.-K.K. All authors have read and agreed to the published version of the manuscript.

Funding: This research was supported by grants from the National Research Foundation of the Republic of Korea (NRF) grant funded by the Korean government (MSIT) (No. 2020R1A2C1004355; No. 2022R1F1A1062766).

Institutional Review Board Statement: This study was conducted in accordance with the Declaration of Helsinki, and approved by the Institutional Review Board (or Ethics Committee) of Gachon University (IRB No. 1044396-202105-HR-105-01).

Informed Consent Statement: Informed consent was obtained from all participants involved in the study.

Data Availability Statement: The data presented in this study are available upon request from the corresponding author.

Acknowledgments: This experiment was conducted at the Gachon University Medical Campus.

Conflicts of Interest: The authors declare that they have no competing financial interests or personal relationships that may have influenced the work reported in this study.

References

1. Manbachi, A.; Cobbold, R.S.C. Development and Application of Piezoelectric Materials for Ultrasound Generation and Detection. *Ultrasound* **2011**, *19*, 187–196. [CrossRef]
2. Madsen, E.L.; Frank, G.R.; Dong, F. Liquid or Solid Ultrasonically Tissue-Mimicking Materials with Very Low Scatter. *Ultrasound Med. Biol.* **1998**, *24*, 535–542. [CrossRef]
3. Chan, V.; Perlas, A. Basics of Ultrasound Imaging. In *Atlas of Ultrasound-Guided Procedures in Interventional Pain Management*; Narouze, S.N., Ed.; Springer: New York, NY, USA, 2011; pp. 13–19, ISBN 978-1-4419-1681-5.
4. Aldrich, J.E. Basic Physics of Ultrasound Imaging. *Crit. Care Med.* **2007**, *35*, S131–S137. [CrossRef]
5. Chen, Q.; Zagzebski, J.A. Simulation Study of Effects of Speed of Sound and Attenuation on Ultrasound Lateral Resolution. *Ultrasound Med. Biol.* **2004**, *30*, 1297–1306. [CrossRef] [PubMed]
6. Zhang, Z.; Liu, M.; Li, Q.; Png, M. Baseline-Free Defect Evaluation of Complex-Microstructure Composites Using Frequency-Dependent Ultrasound Reflections. *Compos. Part A Appl. Sci. Manuf.* **2020**, *139*, 106090. [CrossRef]
7. Chapman, A.; ter Haar, G. Thermal Ablation of Uterine Fibroids Using MR-Guided Focused Ultrasound-a Truly Non-Invasive Treatment Modality. *Eur. Radiol.* **2007**, *17*, 2505–2511. [CrossRef] [PubMed]
8. Scholz, A.M.; Bünger, L.; Kongsro, J.; Baulain, U.; Mitchell, A.D. Non-Invasive Methods for the Determination of Body and Carcass Composition in Livestock: Dual-Energy X-ray Absorptiometry, Computed Tomography, Magnetic Resonance Imaging and Ultrasound: Invited Review. *Animal* **2015**, *9*, 1250–1264. [CrossRef] [PubMed]
9. Heckmatt, J.Z.; Pier, N.; Dubowitz, V. Real-Time Ultrasound Imaging of Muscles. *Muscle Nerve* **1988**, *11*, 56–65. [CrossRef] [PubMed]
10. Whittaker, J.L.; Stokes, M. Ultrasound Imaging and Muscle Function. *J. Orthop. Sports Phys. Ther.* **2011**, *41*, 572–580. [CrossRef] [PubMed]
11. Saul, T.; Siadecki, S.D.; Berkowitz, R.; Rose, G.; Matilsky, D.; Sauler, A. M-Mode Ultrasound Applications for the Emergency Medicine Physician. *J. Emerg. Med.* **2015**, *49*, 686–692. [CrossRef] [PubMed]
12. Quiñones, M.A.; Otto, C.M.; Stoddard, M.; Waggoner, A.; Zoghbi, W.A. Recommendations for Quantification of Doppler Echocardiography: A Report from the Doppler Quantification Task Force of the Nomenclature and Standards Committee of the American Society of Echocardiography. *J. Am. Soc. Echocardiogr.* **2002**, *15*, 167–184. [CrossRef]
13. Quistgaard, J.U. Signal Acquisition and Processing in Medical Diagnostic Ultrasound. *IEEE Signal Process. Mag.* **1997**, *14*, 67–74. [CrossRef]
14. Park, R.; Nyland, T.; Lattimer, J.; Miller, C.; Lebel, J. B-Mode Gray-Scale Ultrasound: Imaging Artifacts and Interpretation Principles. *Vet. Radiol.* **1981**, *22*, 204–210. [CrossRef]
15. Reusz, G.; Sarkany, P.; Gal, J.; Csomos, A. Needle-Related Ultrasound Artifacts and Their Importance in Anaesthetic Practice. *Br. J. Anaesth.* **2014**, *112*, 794–802. [CrossRef]
16. Xiao, G.; Brady, M.; Noble, J.A.; Zhang, Y. Segmentation of Ultrasound B-Mode Images with Intensity Inhomogeneity Correction. *IEEE Trans. Med. Imaging* **2002**, *21*, 48–57. [CrossRef] [PubMed]
17. Gunabushanam, G.; Scoutt, L.M. Ultrasound Image Optimization for the Interventional Radiologist. *Tech. Vasc. Interv. Radiol.* **2021**, *24*, 100766. [CrossRef] [PubMed]
18. Klucinec, B. The Effectiveness of the Aquaflex Gel Pad in the Transmission of Acoustic Energy. *J. Athl. Train.* **1996**, *31*, 313–317. [PubMed]
19. Jhu, J.-L.; Chai, H.-M.; Jan, M.-H.; Wang, C.-L.; Shau, Y.-W.; Wang, S.-F. Reliability and Relationship between 2 Measurements of Transversus Abdominis Dimension Taken during an Abdominal Drawing-in Maneuver Using a Novel Approach of Ultrasound Imaging. *J. Orthop. Sports Phys. Ther.* **2010**, *40*, 826–832. [CrossRef] [PubMed]
20. Mohamed, A.S.A. *Automated Speckle Tracking in Ultrasound Images of Tendon Movements*; University of Salford: Salford, UK, 2014.
21. Hicks, K.M.; Onambélé, G.L.; Winwood, K.; Morse, C.I. Muscle Damage Following Maximal Eccentric Knee Extensions in Males and Females. *PLoS ONE* **2016**, *11*, e0150848. [CrossRef] [PubMed]
22. Park, C.; Cho, H.-Y.; Kang, C.-K. Investigation of Structural Changes in Rectus Abdominis Muscle According to Curl-Up Angle Using Ultrasound with an Extended Field of View. *Int. J. Environ. Res. Public Health* **2022**, *19*, 14525. [CrossRef]

23. Hatjipetrou, A.; Anyfantakis, D.; Kastanakis, M. Rectus Sheath Hematoma: A Review of the Literature. *Int. J. Surg.* **2015**, *13*, 267–271. [CrossRef]
24. Gatt, A.; Agarwal, S.; Zito, P.M. Anatomy, Fascia Layers. In *StatPearls*; StatPearls Publishing: Treasure Island, FL, USA, 2024.
25. Kubo, K.; Kanehisa, H.; Fukunaga, T. Comparison of Elasticity of Human Tendon and Aponeurosis in Knee Extensors and Ankle Plantar Flexors in Vivo. *J. Appl. Biomech.* **2005**, *21*, 129–142. [CrossRef]
26. Malliaras, P.; Kamal, B.; Nowell, A.; Farley, T.; Dhamu, H.; Simpson, V.; Morrissey, D.; Langberg, H.; Maffulli, N.; Reeves, N. Patellar Tendon Adaptation in Relation to Load-Intensity and Contraction Type. *J. Biomech.* **2013**, *46*, 1893–1899. [CrossRef]
27. Bohm, S.; Mersmann, F.; Schroll, A.; Mäkitalo, N.; Arampatzis, A. Insufficient Accuracy of the Ultrasound-Based Determination of Achilles Tendon Cross-Sectional Area. *J. Biomech.* **2016**, *49*, 2932–2937. [CrossRef]
28. Selfridge, A.R. Approximate Material Properties in Isotropic Materials. *IEEE Trans. Son. Ultrason.* **1985**, *32*, 381–394. [CrossRef]
29. Maganaris, C.N.; Paul, J.P. Hysteresis Measurements in Intact Human Tendon. *J. Biomech.* **2000**, *33*, 1723–1727. [CrossRef]
30. Morsink, C.F.; Dam-Vervloet, A.J.; Krommendijk, M.E.; Kaya, M.; Cuartas-Vélez, C.; Knop, T.; Francis, K.J.; Bosschaart, N. Design and Characterization of Color Printed Polyurethane Films as Biomedical Phantom Layers. *Biomed. Opt. Express* **2023**, *14*, 4485. [CrossRef] [PubMed]
31. Badiuk, S.R.; Sasaki, D.K.; Rickey, D.W. An Anthropomorphic Maxillofacial Phantom Using 3-Dimensional Printing, Polyurethane Rubber and Epoxy Resin for Dental Imaging and Dosimetry. *Dentomaxillofac. Radiol.* **2022**, *51*, 20200323. [CrossRef] [PubMed]
32. Banks, V.; Bale, S.; Harding, K.; Harding, E.F. Evaluation of a New Polyurethane Foam Dressing. *J. Wound Care* **1997**, *6*, 266–269. [CrossRef] [PubMed]
33. Morales-González, M.; Díaz, L.E.; Dominguez-Paz, C.; Valero, M.F. Insights into the Design of Polyurethane Dressings Suitable for the Stages of Skin Wound-Healing: A Systematic Review. *Polymers* **2022**, *14*, 2990. [CrossRef] [PubMed]
34. Basseal, J.M.; Westerway, S.C.; Hyett, J.A. Analysis of the Integrity of Ultrasound Probe Covers Used for Transvaginal Examinations. *Infect. Dis. Health* **2020**, *25*, 77–81. [CrossRef]
35. Gupta, M.; Taneja, H.; Chand, L. Performance Enhancement and Analysis of Filters in Ultrasound Image Denoising. *Procedia Comput. Sci.* **2018**, *132*, 643–652. [CrossRef]
36. Vimala, B.B.; Srinivasan, S.; Mathivanan, S.K.; Muthukumaran, V.; Babu, J.C.; Herencsar, N.; Vilcekova, L. Image Noise Removal in Ultrasound Breast Images Based on Hybrid Deep Learning Technique. *Sensors* **2023**, *23*, 1167. [CrossRef]
37. Ghali, S.; Katti, G.; Shahbaz, S.; Chitroda, P.K.; Anukriti, V.; Divakar, D.D.; Khan, A.A.; Naik, S.; Al-Kheraif, A.A.; Jhugroo, C. Fascial Space Odontogenic Infections: Ultrasonography as an Alternative to Magnetic Resonance Imaging. *World J. Clin. Cases* **2021**, *9*, 573–580. [CrossRef]
38. Duitama, I.G.; Claramunt, A.A.; Gonzalez, P.G. Muscles and Fasciae. In *Elastography of the Musculoskeletal System*; Marsico, S., Solano, A., Eds.; Springer International Publishing: Cham, Switzerland, 2023; pp. 79–97, ISBN 978-3-031-31054-6.
39. Mast, T.D.; Hinkelman, L.M.; Orr, M.J.; Sparrow, V.W.; Waag, R.C. Simulation of Ultrasonic Pulse Propagation through the Abdominal Wall. *J. Acoust. Soc. Am.* **1997**, *102*, 1177–1190. [CrossRef]
40. Adstrum, S.; Hedley, G.; Schleip, R.; Stecco, C.; Yucesoy, C.A. Defining the Fascial System. *J. Bodyw. Mov. Ther.* **2017**, *21*, 173–177. [CrossRef] [PubMed]
41. Niraj, G. Pathophysiology and Management of Abdominal Myofascial Pain Syndrome (AMPS): A Three-Year Prospective Audit of a Management Pathway in 120 Patients. *Pain Med.* **2018**, *19*, 2256–2266. [CrossRef] [PubMed]
42. Mohseni-Bandpei, M.A.; Nakhaee, M.; Mousavi, M.E.; Shakourirad, A.; Safari, M.R.; Kashani, R.V. Application of Ultrasound in the Assessment of Plantar Fascia in Patients with Plantar Fasciitis: A Systematic Review. *Ultrasound Med. Biol.* **2014**, *40*, 1737–1754. [CrossRef]
43. Wei, K.; Jayaweera, A.R.; Firoozan, S.; Linka, A.; Skyba, D.M.; Kaul, S. Quantification of Myocardial Blood Flow with Ultrasound-Induced Destruction of Microbubbles Administered as a Constant Venous Infusion. *Circulation* **1998**, *97*, 473–483. [CrossRef]
44. Brannigan, M.; Burns, P.N.; Wilson, S.R. Blood Flow Patterns in Focal Liver Lesions at Microbubble-Enhanced US. *RadioGraphics* **2004**, *24*, 921–935. [CrossRef]
45. Khumri, T.M.; Main, M.L. Safety and Risk–Benefit Profile of Microbubble Contrast Agents in Echocardiography. *Asia Pacif Cardiol.* **2008**, *2*, 47–49. [CrossRef]
46. Ji, X.; Wei, M.; Wang, L.; Li, J.; Gao, D.; Geng, C. Application of Ultrasound-Guided Placement of Markers for Locating Axillary Lymph Nodes of Breast Cancer. *Gland. Surg.* **2021**, *10*, 3067–3074. [CrossRef] [PubMed]
47. Kim, J.H.; Hong, S.S.; Kim, J.H.; Park, H.J.; Chang, Y.-W.; Chang, A.R.; Kwon, S.-B. Safety and Efficacy of Ultrasound-Guided Fiducial Marker Implantation for CyberKnife Radiation Therapy. *Korean J. Radiol.* **2012**, *13*, 307. [CrossRef] [PubMed]
48. Tsoumakidou, G.; Saltiel, S.; Villard, N.; Duran, R.; Meuwly, J.-Y.; Denys, A. Image-Guided Marking Techniques in Interventional Radiology: A Review of Current Evidence. *Diagn. Interv. Imaging* **2021**, *102*, 699–707. [CrossRef] [PubMed]
49. Edeiken, B.S.; Fornage, B.D.; Bedi, D.G.; Singletary, S.E.; Ibrahim, N.K.; Strom, E.A.; Holmes, F. US-Guided Implantation of Metallic Markers for Permanent Localization of the Tumor Bed in Patients with Breast Cancer Who Undergo Preoperative Chemotherapy. *Radiology* **1999**, *213*, 895–900. [CrossRef]